

Y. LIU¹, Y. ZHAO¹, J. GUAN^{1*}, Y. YANG^{2**}, J. ZHU¹**TIG WELDING CRACK SENSIBILITY ANALYSIS OF Co-BASED SUPERALLOYS**

The microstructure of alloy phases and hot crack propagation under TIG (tungsten inert gas) welding of Co-based superalloys are investigated. The μ -phase, β -phase and carbides are grown in the superalloy, and the μ -phase is mainly precipitated. The microhardness of the μ phase is higher than the β phase and the matrix. During TIG welding, the arc crater cracks in the molten pool are all intergranular. The equiaxed crystals are existed in the fusion zone, and the dendrites are appeared in the heat affected zone. The microcracks in the heat-affected zone and closed to the base metal are preferentially initiated in the region of the μ phase, and continuously extend to the matrix along the growth direction of the μ phase.

Keywords: Superalloy; TIG welding; Alloy phase; Crack propagation

1. Introduction

Co-based superalloys have been widely used in aerospace, marine engineering and chemical industries because they have more excellent high temperature properties, corrosion resistance and weldability than nickel-based alloys [1]. Welding is the most effective method for joining complex superalloy components and repairing tiny defects formed during casting and service [2]. Thus, the usability is greatly limited.

For example, some nickel-based superalloys, especially those with high Al and Ti content (Al/Ti > 6 wt.%), are easy to form solidification cracks, liquefaction cracks and strain aging cracks. This makes them be considered non-weldable and their application is limited [3-5]. An effective way to improve the properties of superalloys is to increase the content of refractory alloying elements [6]. However, more refractory elements in alloys tend to promote the formation of topological compact stacking phases (TCP). The formation of TCP phase is mainly caused by element diffusion [7], which is closely related to temperature, time and stress [8-9]. The presence of the phase would seriously damage the strengthening elements of the superalloys and lead to the formation of cracks caused by local stress concentration [10-11]. From a mechanical point of view, the TCP phase is a brittle inclusion, which will significantly reduce the service life of Ni-based single crystals. TCP phase, such as μ phase, is highly ordered phase in terms of packing [12].

It generally precipitates in the alloys. Due to its different morphology, the μ phase has different effects on the properties of superalloys [13-14]. Spherical μ -phase precipitates are prone to debonding, while needle-like or sheet-like precipitates lead to dislocation stacking and cracking. Their complex crystal structure usually results in significant brittleness of these phases, which is easy to form crack source. Hong et al. [15] reported that microcracks initiation in the heat-affected zone of Inconel 718 welded joints were reduced the fatigue life of welded joints, while the relationship between welding crack and TCP phase is not clearly explained.

In the paper, the Co-based superalloy is carried out by TIG spot welding, and the behavior of welding crack initiation and propagation is analyzed. The microstructure and the characterization of alloy phase are discussed. The relationship between cracks generated during TIG welding and TCP phase growth is illustrated.

2. Experimental procedure

The chemical composition of the experimental material Co base superalloy is shown in TABLE 1. The superalloy specimens were subjected to conventional wire cutting. The samples were mechanically ground and polished with a series of silicon carbide abrasive papers to obtain the mirror finish required

¹ LIAONING PETROCHEMICAL UNIVERSITY, SCHOOL OF MECHANICAL ENGINEERING, FUSHUN 113001, CHINA

² CHINESE ACADEMY OF SCIENCES, INSTITUTE OF METAL RESEARCH SHENYANG 110016, CHINA

Corresponding authors: * guanjianjun@lnpu.edu.cn; ** yhyang@imr.ac.cn



Chemical composition of Co-based superalloy (wt.%)

Element	Al	W	Ni	Cr	Ta	Hf	Ti	C	B	Mo	Co
	4.0	10.0	30.0	5.0	8.0	1.5	2.0	0.050	0.024	5.0	Bal.

for metallographic analysis, degreased with alcohol and cleaned with distilled water and acetone with ultrasonic. The samples were electrolytically etched in the corrosive solution of $42\%H_3PO_4 + 34\%H_2SO_4 + 24\%H_2O$.

The morphology was observed and the quantitative analysis was detected on the micro areas of the material, by means of metallographic microscope, backscatter electron (BSE) mode and the secondary electron (SE) mode of scanning electron microscope (SEM) combined with energy dispersive spectrometer (EDS). The phase structure was identified by X-ray diffraction (XRD). The area fraction of the phase was calculated using Image Pro Plus software. The hardness of each phase was evaluated by vickers microhardness test. The sample with diameter of 16 mm and thickness of 2 mm shall be subjected to TIG spot welding. BSE analysis of thermal crack propagation after welding was carried out by scanning electron microscope (SEM). The welding process and SEM equipment is shown in Fig. 1.

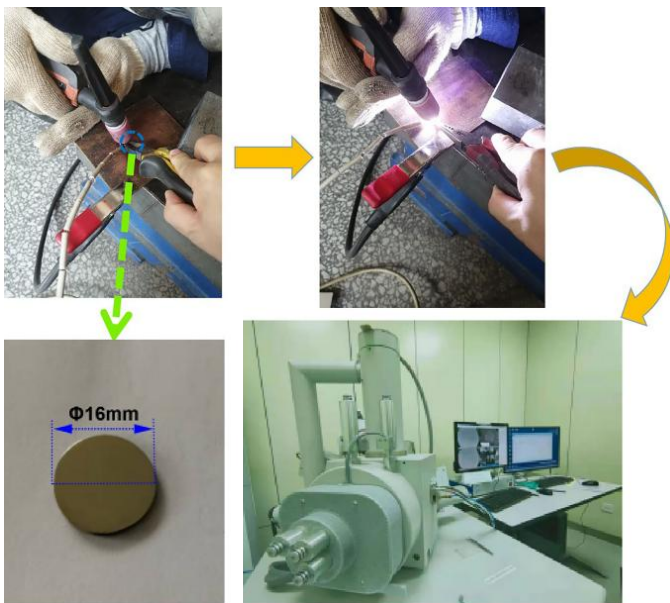


Fig. 1. Welding process diagram

3. Results and discussion

3.1. Microstructure of the experimental alloy

As shown in Fig. 2, the diffraction peaks in the XRD of the Co-based superalloy can clearly show the μ phase and the matrix γ . The superalloy morphology is microscopically observed by SEM in BSE mode. Fig. 3 shows the morphology of the experimental alloy. In Fig. 3(a), distinct contrast phase, dark gray phase, light gray phase and bright carbides are observed in the interdendritic region. From results of phase composition with

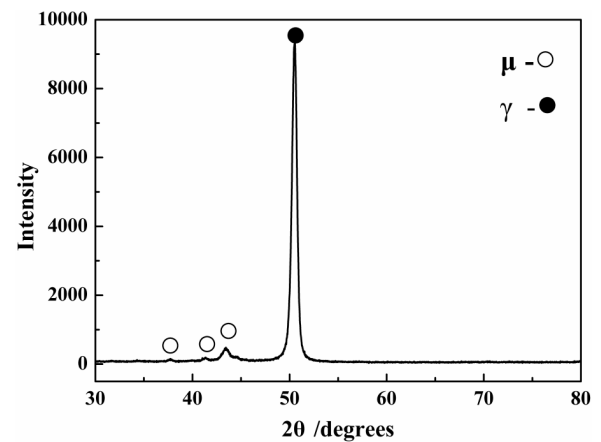


Fig. 2. XRD analysis results of Co-based superalloy

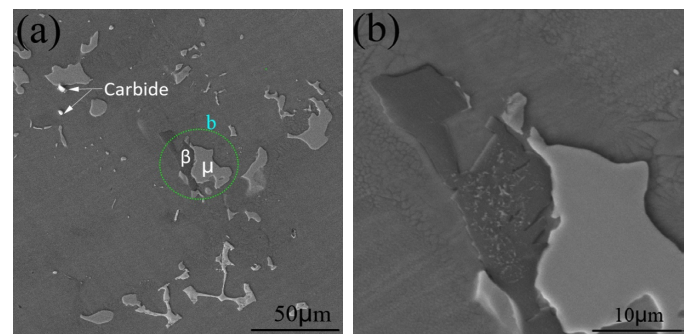


Fig. 3. (a) Microstructure of Co-based superalloy, (b) Magnified morphology of the circle in (a)

EDS, it is known that the light gray phase is rich in W and Mo elements, and the dark gray phase is rich in Al elements. The light gray phases are Co_3W or Co_7W_6 (also known as μ phase), and the dark gray phase is Al-Co (also known as β phase) [16-18]. Fig. 4 shows the chemical elemental segregation in each phase using the EDS mapping analysis. Fig. 4(a) shows the measured region morphology, and Fig. 4(b) shows the distribution of the corresponding Al-rich elements in the β region. Fig. 4(c) shows the distribution map of the μ region rich in the corresponding W element. Fig. 4(d) shows the distribution of the corresponding Mo elements enriched in the μ region.

Fig. 5 shows the metallographic morphology of Co-based superalloy. The area fraction of μ phase and β phase is calculated by Image Pro Plus software. The 15 sheets under the 200-fold metallographic are used for the phase fraction calculation. The calculation results are shown in Fig. 6. The proportion of μ phase is 19.1%, and the proportion of β phase is 2.2%. The volume fraction of β phase is lower, so it does not appear in XRD tests. The μ phase is a kind of topologically dense phase, which is famous for its complex crystal structure and physical properties. The μ phase has the ideal STOichiometry of A_6B_7 , and its

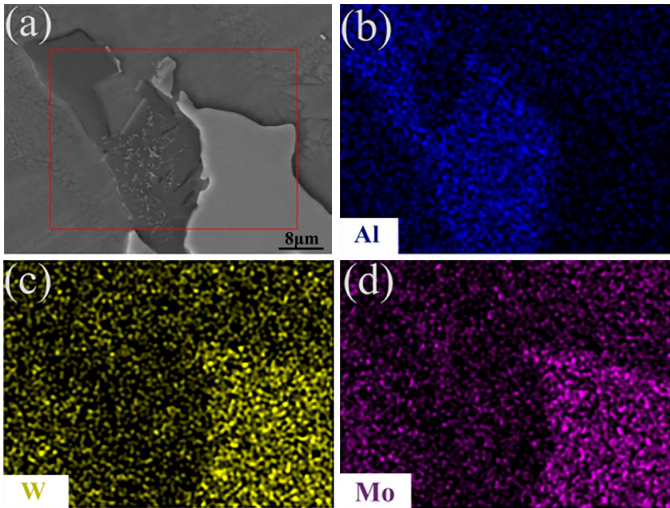


Fig. 4. EDS mapping results of each phase in the experiment alloys, (a) morphology, (b) (c) (d) element distribution

prototype is Fe_7W_6 with a rhombohedral cell of 13 atoms [19]. Due to the high volume fraction of the μ phase, its properties easily affect the mechanical properties and ductility.

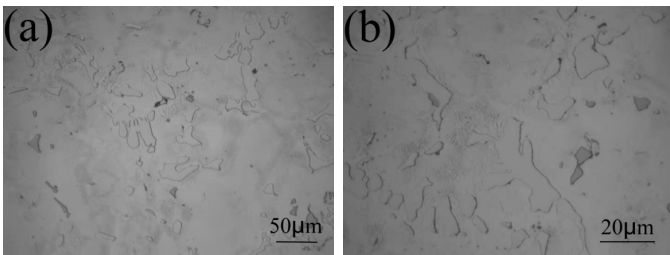


Fig. 5. Metallographic morphology of Co-based superalloy, (a) 200 \times , (b) 500 \times

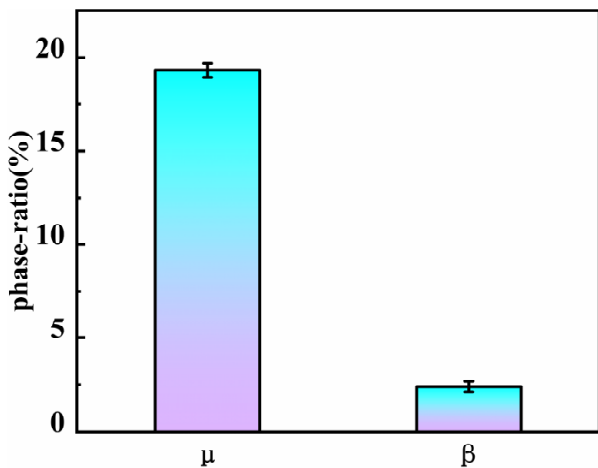


Fig. 6. Area fraction of each phase in the experimental alloy (%)

3.2. Morphology after welding

The molten pool after welding is mainly divided into three parts, namely fusion zone, heat Affected zone and base metal. These three parts can be observed, and the morphology is shown

in Fig. 7(a). A region is fusion zone, B region is heat affected zone, and C region is base metal. Fig. 7(b) is a schematic diagram of the post-weld morphology simulated by ANSYS one-to-one scale, which includes the fusion zone (FZ), the heat-affected zone (HAZ) and the base metal (BM).

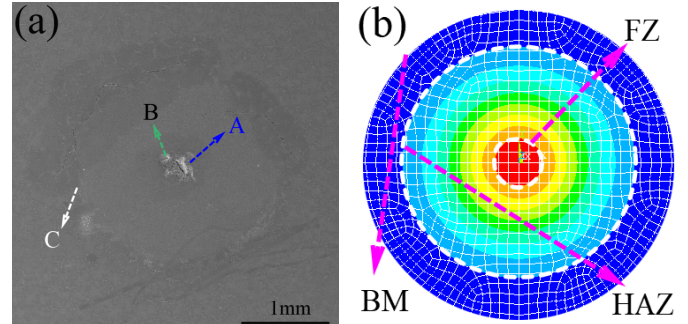


Fig. 7. (a) Morphology of welding pool, (b) regional distribution of BM, HAZ and FZ in numerical simulation

The TIG welding is employed on the superalloy, and the welding molten pool microstructure is shown in Fig. 8. In Fig. 8(a), obvious crater cracks in the fusion zone is observed. There are fine cracks in the heat affected zone. The macroscopic cracks are caused by the large heat input. In Fig. 8(b), the small cracks are appeared in the heat-affected zone, which are intergranular cracking. In Fig. 8(c), fine cracks pass through the μ phase between the base metal and the heat-affected zone. The magnified morphology is shown in Fig. 8(d), as circled in Fig. 8(a). It is observed that the equiaxed crystals are grown in the fusion zone, and the dendrites are grown in the heat-affected

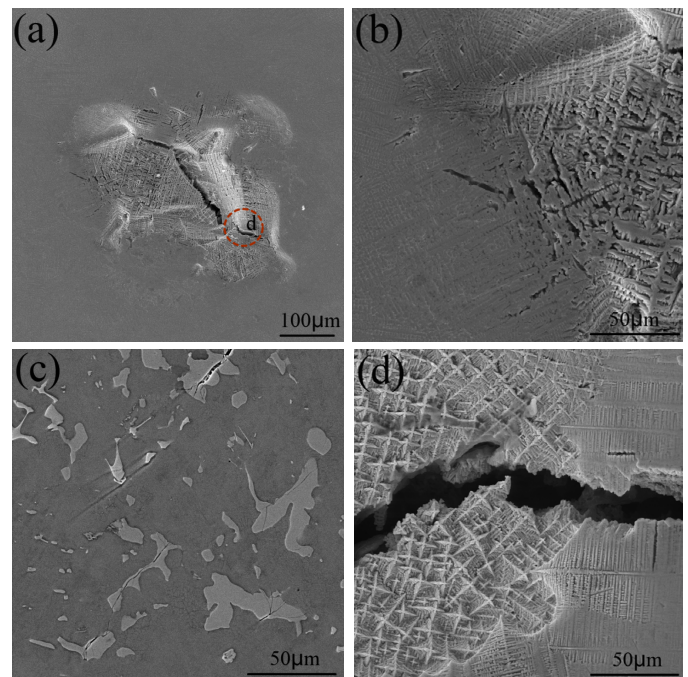


Fig. 8. Crack distribution in the welding region. (a) Macro cracks, (b) Crack distribution in the fusion zone close to the heat-affected zone, (c) Crack distribution in the heat-affected zone close to the base metal, (d) Solidification structure in the fusion zone

zone. The cracks are intergranular. The metal melts during the welding process, and the heat generated by the arc is continuously transferred outward through the molten pool. At this time, the liquid metal in the molten pool is in a state of overheating. There is a positive temperature gradient at the solid-liquid interface. During the solidification process of the alloy, it is different for the diffusion coefficients of solute atoms in the solid and liquid phases. With the continuous advancement of the solidification process, the composition supercooling phenomenon will occur. Canada's physical metallurgist Professor B. Chalmers and his research group put forward the concept of interface stability and the famous theoretical component supercooling theory [20]. Its judgment is based on the following Formula (1).

$$\frac{G}{R} \geq \frac{m_L C_0 (k-1)}{k D_L} = \frac{\Delta T_0}{D_L} \quad (1)$$

Nowadays, the theory of composition supercooling has been confirmed by many experiments. When G/R is less to a certain range, a larger number of crystal nuclei are formed at the solid-liquid interface, and crystal nuclei grow up continuously in the form of equiaxed crystals. The composition subcooling theory considers that the influence of temperature gradient and concentration gradient on the interface can be convenient to analyze the influence of solidification on the crystal morphology under certain conditions. During the welding process, there is a sub-cooling zone in the molten pool as shown in the Formula (2):

$$\frac{G}{R} < \frac{m_L c_0 (k-1)}{k_0 D_l} = \frac{\Delta T_0}{D_l} \quad (2)$$

In the above formula, ΔT_0 is the solidification temperature range, G is the temperature gradient, R represents the advancing speed of the solid-liquid interface, m_L is the slope of the liquidus line in the phase diagram, k represents the equilibrium distribution coefficient, D_l is the diffusion coefficient of the solute in the liquid phase. During the solidification of the weld pool, the size of the component undercooling will ultimately determine the solidified microstructure and morphology. The temperature gradient G and the advancing speed R of the interface can impact on the microstructure and grain size of the solidified alloy. With the decreasing G/R ratio, the solidification microstructure underwent the transition from planar crystal to cellular crystal to columnar dendritic crystal to equiaxed dendritic crystal. In the actual welding molten pool, the ratio of G/R is different in the positions, and the distribution of the solidification structure in the weld in the experiment results is also uneven [21]. At the boundary of the welding pool, the temperature gradient is higher, and the crystallization speed is lower. It is difficult to generate the constitutional supercooling phenomenon. The crystals gradually grow towards the central fusion zone of the molten pool. The temperature gradient decreases from the edge of the molten pool to the center, and the crystallization speed gradually increases. The solute content increases, and the constitutional supercooling gradually increases. The microstructure of the crystals changed from cellular to columnar to equiaxed dendrites in turn. In the

middle melting region of the molten pool, the change of temperature gradient is the smallest, and the speed of crystallization is the highest. The phenomenon of constitutional supercooling resulted in the formation of equiaxed grains. Its growth trend is shown in Fig. 9.

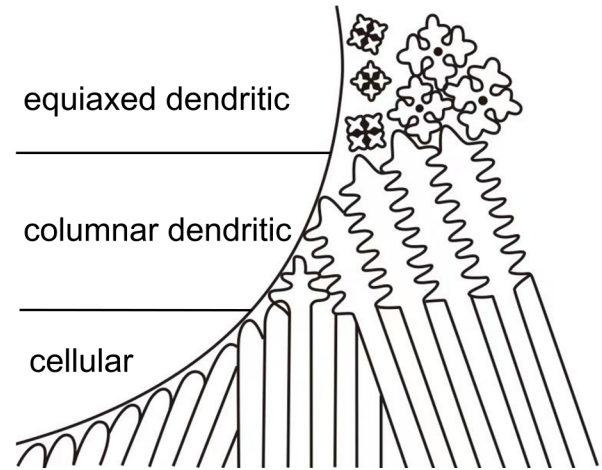


Fig. 9. Crystallization structure distribution of solidification process [22]

3.3. Crack propagation in phases

The precipitation of the topologically close-packed phase will destroy the stability of the alloy structure. Spherical μ -phase precipitates are prone to debonding, while needle-like or sheet-like precipitates can lead to dislocation stacking and cracking [22]. The μ phase in the experimental alloys is flaky (Fig. 3). The welding crack propagation morphology are shown in Fig. 10. Fig. 10(a) shows that the hot cracks are concentrated between the heat-affected zone and the base metal. Microcracks at the edge of the base metal in the heat affected zone can be caused by welding residual stress, which further reduces the service life of the alloy. In Fig. 8(c), the cracks preferentially appear in the μ phase with flakes, and the angles of these cracks vary from 20° to 85° . These distinct cracks are observed only in the μ phase. These microcracks on the μ phase show a tendency to propagate from the μ phase to the matrix. Crack propagates pass through the μ phase to the matrix, as shown in Fig. 10(b). The crack penetrates the μ phase and extends to the next μ phase of the matrix, and finally generates the macroscopic crack. In Fig. 10(c), the cracks on the μ phase continuously expand along the growth direction of μ phase. The crack on μ phase is wider than that on matrix, and the crack propagation path is serrated. The precipitation of μ phase will destroy the stability of the superalloy structure.

The hardness tests of each phase and matrix of the experimental alloy are carried out, and the results are shown in Fig. 11. The microhardness of the μ phase is the highest, followed by β phase and the matrix γ phase. There is a correlation between material hardness and its brittleness. The greater the hardness is, the greater the brittleness is. The μ phase has a higher microhardness, and the crack is easier initiated and propagated

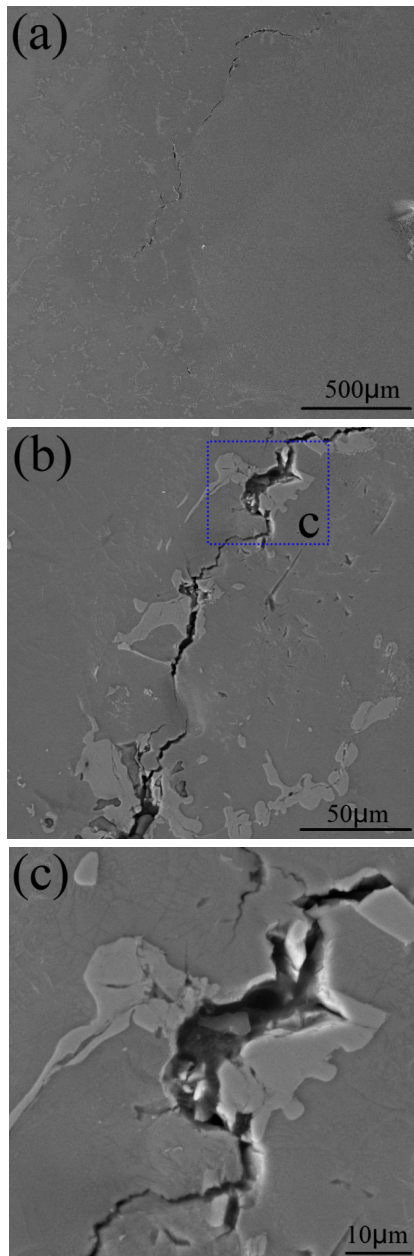


Fig. 10. (a) Cracks near the base metal in the heat affected zone, (b) Magnified morphology of (a), (c) Magnified morphology of (b)

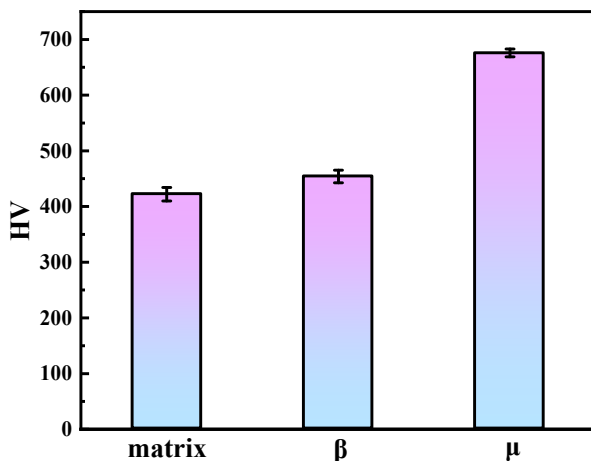


Fig. 11. Micro Vickers hardness of each phase in the superalloy

in the phase. This further clarifies that the microcracks in the heat-affected zone close to the base metal preferentially appear in the μ phase and continue to expand along the growth direction of the μ phase.

4. Conclusions

- (1) The microstructure is observed for Co-based superalloy, and the μ -phase, β -phase and carbides are found. The μ phase is presented as a light gray block morphology, and it is rich in W and Mo elements. The β phase is presented as a dark gray block morphology, and it is rich in Al element. The carbide appears as the white and bright polyhedron.
- (2) Co-based superalloy is carried out by TIG welding. The melting zone in the molten pool exists in the form of equiaxed crystals, and the heat-affected zone exists in the form of dendrites. Crater cracks due to heat input crack grow along the equiaxed and dendritic grain boundaries.
- (3) In TIG welding, the microcracks in the heat-affected zone are preferentially initiated in the μ phase and continue to expand along the growth direction of μ phase. The crack propagation path is along zigzag propagation. The microhardness of the μ phase is higher than the β phase and the matrix, and the crack is easier initiated and propagated along the μ phase.

Acknowledgements

This work was supported by Basic scientific research projects of colleges and universities of Liaoning Provincial Department of Education (No. LJKMZ20220753), National Key R&D Program of China under Grant (No. 2021YFB3700401), and Liaoning Provincial Student's Platform for Innovation and Entrepreneurship Training Program (No. S202310148028).

REFERENCES

- [1] E.A. Lass, D.J. Souza, D.C. Dnand, D.N. Seidman, Multicomponent γ' -strengthened Co-based superalloys with increased solvus temperatures and reduced mass densities. *Acta Mater.* **147**, 284-295 (2018). DOI: <https://doi.org/10.1016/j.actamat.2018.01.034>
- [2] R. Kataria, R.P. Singh, P. Sharma, R.K. Phanden, Welding of super alloys: A review. *Mater. Today* **38**, 265-268 (2021). DOI: <https://doi.org/10.1016/j.matpr.2020.07.198>
- [3] M.J. Xie, Y. Zhao, J.J. Guan, Y.H. Yang, Y.T. Fu, Influence of Carbon Additions on Microstructures and Mechanical Properties in Additive Manufactured Superalloys. *Mater. Adv.* **4**, 4897-4912 (2023). DOI: <https://pubs.rsc.org/en/content/articlelanding/2023/ma/d3ma00370a>
- [4] M.K. Keshavarz, S. Turenne, A. Bonakdar, Solidification behavior of inconel 713LC gas turbine blades during electron beam welding. *J. Manuf. Processes* **31**, 232-239 (2018). DOI: <https://doi.org/10.1016/j.jmapro.2017.11.021>

- [5] Y. Lei, K. Aoyagi, K. Aota, K. Kuwabara, A. Chiba, Critical factor triggering grain boundary cracking in non-weldable superalloy Alloy713ELC fabricated with selective electron beam melting. *Acta Mater.* **208**, 116695-116702 (2021). DOI: <https://doi.org/10.1016/j.actamat.2021.116695>
- [6] C. Barbosa, J.L. Nascimento, I.M.V. Caminha, I.C. Abud, Microstructural aspects of the failure analysis of nickel base superalloys components. *Eng. Fail. Analysis* **12**, 348-361 (2005). DOI: <https://doi.org/10.1016/j.engfailanal.2004.09.010>
- [7] W.S. Xia, X.B. Zhao, L. Yue, Z. Zhang, Microstructural evolution and creep mechanisms in Ni-based single crystal superalloys: A review. *J. Alloy Comp.* **819**, 152954-152989 (2020). DOI: <https://doi.org/10.1016/j.jallcom.2019.152954>
- [8] J.J. Huo, Q.Y. Shi, Y.R. Zheng, Q. Feng, Microstructural nature and stability of Co-rich TCP phases in Ru-containing single crystal superalloys. *J. Alloy Comp.* **715**, 460-470 (2017). DOI: <https://doi.org/10.1016/j.jallcom.2017.05.015>
- [9] X.L. Li, W. Li, M.I. Lashari, T. Sakai, P. Wang, L. Cai, X.M. Ding, U. Hamid, Fatigue failure behavior and strength prediction of nickel-based superalloy for turbine blade at elevated temperature. *Eng. Fail. Analysis* **136**, 106191-106204 (2022). DOI: <https://doi.org/10.1016/j.engfailanal.2022.106191> 610 (2014) 589e593
- [10] J.X. Sun, J.L. Liu, J.G. Li, C. Chen, X.G. Wang, Y.L. Zhou, X.F. Xiao, Dual effects of Ru on the microstructural stability of a single crystal superalloy. *Scripta Mater.* **205**, 114209-114213 (2021). DOI: <https://doi.org/10.1016/j.scriptamat.2021.114209>
- [11] J. Liu, J.J. Yu, Y.H. Yang, Y.Z. Zhou, X.F. Sun, Effects of Mo on the evolution of microstructures and mechanical properties in Co-Al-W base superalloys. *Mater. Sci. Eng. A* **745**, 404-410 (2019). DOI: <https://doi.org/10.1016/j.msea.2018.11.087>
- [12] W.P. Huhn, M. Widom, A.M. Cheung, G.J. Shiflet, S.J. Poon, J. Lewandowski, First-principles calculation of elastic moduli of early-late transition metal alloys. *Phys. Rev. B* **89**, 104103-104108 (2014). DOI: <https://doi.org/10.1103/PhysRevB.89.104103>
- [13] Y.X. Chen, G.L. Wang, J.D. Liu, L.L. He, Atomic configurations of planar defects in μ phase in Ni-based superalloys. *Scripta Mater.* **193**, 27-32 (2021). DOI: <https://doi.org/10.1016/j.scriptamat.2020.09.045>
- [14] H. Rehman, K. Durst, S. Neumeier, A.B. Parsa, A. Kostka, G. Eggeler, M. Goken, Nanoindentation studies of the mechanical properties of the μ phase in a creep deformed Re containing nickel-based superalloy. *Mater. Sci. Eng. A* **634**, 202-208 (2015). DOI: <https://doi.org/10.1016/j.msea.2015.03.045>
- [15] S.L. Kwon, S.H. Bae, J.H. Do, C.Y. Jo, H.U. Hong, Characterization of the Microstructures and the Cryogenic Mechanical Properties of Electron Beam Welded Inconel 718. *Metall. Mater. Trans. A* **47**, 777-787 (2016). DOI: <https://doi.org/10.1007/s11661-015-3269-6>
- [16] C.H. Chu, C. Li, Y. Guan, Y.C. Liu, Microstructure-dependent coarsening behavior of γ' precipitates in CoNi-based superalloys. *Intermetallics* **140**, 107396-107403 (2022). DOI: <https://doi.org/10.1016/j.intermet.2021.107396>
- [17] P.A. Carvalho, H.S.D. Haarsma, B.J. Kooi, P.M. Bronsveld, J.ThM. De Hosson, HRTEM study of Co7W6 and its typical defect structure. *Acta Mater.* **48**, 2703-2712 (2000). DOI: [https://doi.org/10.1016/S1359-6454\(00\)00064-1](https://doi.org/10.1016/S1359-6454(00)00064-1)
- [18] J. Liu, J.J. Yu, Y.H. Yang, Y.Z. Zhou, X.F. Sun, Effects of Mo on the evolution of microstructures and mechanical properties in Co-Al-W base superalloys. *Mater. Sci. Eng. A* **745**, 404-410 (2019). DOI: <https://doi.org/10.1016/j.msea.2018.11.087>
- [19] L.R. Liu, B.X. Zhou, Q.F. Wang, Y.H. Yang, J.J. Yu, B.Z. Sun, Intergrowth structure of Laves within μ phases in Co-Al-W base superalloy. *J. Alloy Comp.* **844**, 155822-155830 (2020). DOI: <https://doi.org/10.1016/j.jallcom.2020.155822>
- [20] W.A. Tiller, K.A. Jackson, J.W. Rutter, B. Chalmers, The Redistribution of Solute Atoms during the Solidification of Metals. *Acta Metall.* **1**, 428-437 (1953). DOI: [https://doi.org/10.1016/0001-6160\(53\)90126-6](https://doi.org/10.1016/0001-6160(53)90126-6)
- [21] F. Nematzadeh, M.R. Akbarpour, S. Parvizi, A.H. Kokabi, S.K. Sadmezhaad, Effect of welding parameters on microstructure, mechanical properties and hot cracking phenomenon in udimet 520 superalloy. *Mater. Des.* **36**, 94-99 (2012). DOI: <https://doi.org/10.1016/j.matdes.2011.10.020>
- [22] H. Xu, Y.H. Zhang, H.D. Fu, F. Xue, X.Z. Zhou, J.X. Xie, Effects of boron or carbon on solidification behavior of Co-Ni-Al-W-based superalloys. *J. Alloy Comp.* **891**, 161965-161974 (2022). DOI: <https://doi.org/10.1016/j.jallcom.2021.161965>